View metadata, citation and similar papers at core.ac.uk

brought to you by CORE

provided by Repository@Nottingham

NeuroImage 225 (2021) 117443

Contents lists available at ScienceDirect

NeuroImage

journal homepage: www.elsevier.com/locate/neuroimage

Mouth magnetoencephalography: A unique perspective on the human hippocampus

Tim M. Tierney[a,1,*], Andrew Levy[a,1], Daniel N. Barry[a], Sofie S. Meyer[a,g], Yoshihito Shigihara[b], Matt Everatt[c], Stephanie Mellor[a], Jose David Lopez[d], Sven Bestmann[a], Niall Holmes[e], Gillian Roberts[e], Ryan M Hill[e], Elena Boto[e], James Leggett[e], Vishal Shah[f], Matthew J. Brookes[e], Richard Bowtell[e], Eleanor A. Maguire[a], Gareth R. Barnes[a]

[a] Wellcome Centre for Human Neuroimaging, UCL Queen Square Institute of Neurology, University College London, 12 Queen Square, London WC1N 3AR, UK
[b] Hokuto Hospital MEG Lab, Hokkaido, Japan
[c] S4S (UK) Limited & Smilelign Ltd, 151 Rutland Road, Sheffield S3 9PT, UK
[d] Engineering Faculty, Universidad de Antioquia UDEA, calle 70 No 52-21, Medellín, Colombia
[e] Sir Peter Mansfield Imaging Centre, School of Physics and Astronomy, University of Nottingham, University Park, Nottingham NG7 2RD, UK
[f] QuSpin Inc., 2011 Cherry Street, Unit 112, Louisville, CO 80027, USA
[g] Institute of Cognitive Neuroscience, University College London, 17-19 Queen Square, London WC1N 3AZ, UK

ARTICLE INFO

Keywords:
OPM
MEG
OP-MEG
Hippocampus
Mouth

ABSTRACT

Traditional magnetoencephalographic (MEG) brain imaging scanners consist of a rigid sensor array surrounding the head; this means that they are maximally sensitive to superficial brain structures. New technology based on optical pumping means that we can now consider more flexible and creative sensor placement. Here we explored the magnetic fields generated by a model of the human hippocampus not only across scalp but also at the roof of the mouth. We found that simulated hippocampal sources gave rise to dipolar field patterns with one scalp surface field extremum at the temporal lobe and a corresponding maximum or minimum at the roof of the mouth. We then constructed a fitted dental mould to accommodate an Optically Pumped Magnetometer (OPM). We collected data using a previously validated hippocampal-dependant task to test the empirical utility of a mouth-based sensor, with an accompanying array of left and right temporal lobe OPMs. We found that the mouth sensor showed the greatest task-related theta power change. We found that this sensor had a mild effect on the reconstructed power in the hippocampus (~10% change) but that coherence images between the mouth sensor and reconstructed source images showed a global maximum in the right hippocampus. We conclude that augmenting a scalp-based MEG array with sensors in the mouth shows unique promise for both basic scientists and clinicians interested in interrogating the hippocampus.

1. Introduction

Optically Pumped Magnetometers (OPMs) offer new ways to explore the magnetic fields generated by human brain function. Simulation (Boto et al., 2016; Iivanainen et al., 2017) and empirical recordings (Boto et al., 2017) have shown that it is possible to realize a five-fold signal magnitude increase for cortical sources, simply because OPMs can be placed much closer to the head (with a separation between the sensors' sensitive volume and the scalp of around 6 mm) compared to their cryogenic counterparts (which require a separation of around 17–30 mm). However, for the hippocampus and other sub-cortical structures, the relative change in distance (and hence performance gain) we expect with OPMs over cryogenic systems is smaller - a factor of 2 or less - than for neocortical sources. For this reason, the ability to further leverage the flexibility of OPM-placement to design arrays that are specifically sensitive to these deeper brain areas is desirable.

In this study we exploited the flexibility offered by OPMs to test whether there are other places, besides the scalp surface, one might usefully place sensors. We first examined, in simulation, the topographies of simulated magnetic fields due to hippocampal sources over both the scalp surface and the roof of the mouth. We found that a typical hippocampal generator gave rise to a scalp surface field extremum over the temporal lobe with a corresponding maximum or minimum at the roof of the mouth. We then built a sensor casing into a dental mould and explored the empirical utility of such an arrangement. Using a previously validated hippocampal-dependant task (Barry et al., 2019a), we

* Corresponding author.
E-mail address: tim.tierney.12@ucl.ac.uk (T.M. Tierney).
[1] Equal contribution.

https://doi.org/10.1016/j.neuroimage.2020.117443
Received 3 March 2020; Received in revised form 2 September 2020; Accepted 9 October 2020
Available online 12 October 2020
1053-8119/© 2021 The Authors. Published by Elsevier Inc. This is an open access article under the CC BY license (http://creativecommons.org/licenses/by/4.0/)

assessed the change in theta power across sensors. We then tested the importance of this additional channel for source reconstruction. Finally, we used the temporal lobe array to construct a beamformer image and tested for regions of the brain which were coherent with the mouth channel.

2. Materials and methods

The study had two components, an initial simulation phase followed by the recording and analysis of empirical data.

2.1. Exploring fields due to hippocampal generators

We first used a single participant head-model to explore the field generated across the scalp and over the roof of the mouth by current sources on the hippocampal manifold. We used the individual cortical surface of the participant as extracted from Freesurfer (Dale et al., 1999). For the lead-field modelling, we used an individually segmented hippocampal surface for the single participant, with sources oriented normal to the hippocampal envelope (Meyer et al., 2017). The sources were approximately equally distributed across the entire hippocampal envelope (341 sources, ~2.5 mm separation). The outer scalp and inner-skull meshes were based on the SPM inverse-normalised template meshes (Mattout et al., 2007; Litvak et al., 2011). We assumed the OPMs to be ideal point-source magnetometers with no orientation, position or gain errors. All lead-field calculations were based on the Nolte single-shell forward model (Nolte, 2003). To produce a scalp-level field map for each hippocampal source we computed point estimates that were oriented normal to the outer scalp surface and offset by 6.5 mm from the surface in this direction. This resulted in 2562 samples of external (scalp) field for each source on the hippocampal envelope. Note that for the empirical data, in the next section, the hippocampal geometry was not made use of and the beamfomer sources were reconstructed onto a grid with source orientation at each location chosen to maximise SNR.

2.2. Empirical recordings

2.2.1. Participants

One participant (male, aged 50 years) took part in the study. Data collection took place at the University of Nottingham, UK. The research protocol was approved by the University of Nottingham Medical School Research Ethics Committee and written informed consent was obtained from the participant. The data from the temporal channels of this subject formed part of the cohort of participants reported in (Barry et al., 2019b).

2.2.2. Mouth sensor holder

In order to record from the roof of the mouth, an intraoral appliance to hold the OPM sensor was constructed by S4S (UK) Limited (https://www.s4sdental.com/). Construction started with standard intraoral impressions of the upper and lower dental arches. The appliance (Fig. 1) was constructed from 3 mm Erkoloc-Pro (Erkodent Australia). This is a dual-laminate material composed of two individual thermoplastic layers that are chemically bonded: soft inner layer, helping to improve the comfort of the appliance, and a rigid outer layer that provides stiffness and is able to withstand forces from biting. The appliance was constructed on the upper dental arch which provided a stable base. The use of material with a soft compressible lining enabled us to comfortably engage the majority of the tooth surface while reducing movement and rotation, with minimal risk of the appliance being unremovable. The OPM was fully encapsulated by the appliance to minimise saliva contamination. The dual-laminate material was able to undergo the repeated disinfections needed to ensure hygiene without deterioration.

A limitation on how far into the mouth the appliance can be placed is imposed by the need to avoid activating the gag reflex by impinging on structures in the posterior portion of the oral cavity (soft palate, posterior of tongue, uvula, posterior wall of pharynx, palatoglossal and palatopharyngeal arches). We determined the posterior limit of the appliance to be just anterior of the soft palate. The border of the hard and soft palate is also clearly identifiable both intraorally and radiographically. Based on visual inspection (with approximately ±1 cm of potential error) of the participant's structural MRI brain scan, we estimated the location of the mouth sensor in native space. This corresponded to MNI coordinates $x = -2.4$, $y = 15$, $z = -103$ and the orientation of its sensitive axis in MNI space to be described by the unit vector (0, 0.9885, −0.1513).

2.2.3. Hippocampal-dependant task

We used a task known to be hippocampal-dependant, full details of which are described elsewhere (Barry et al., 2019a). In summary, the experimental task required the imagination of novel scenes in response to single-word cues, and there was an additional baseline condition involving counting. During scanning, experimental stimuli were delivered aurally via an MEG-compatible earbud using the Cogent toolbox (www.vislab.ucl.ac.uk/cogent.php), running in MATLAB. To prepare the participant for each trial type, they first heard either the word "scene" or "counting". The participant immediately closed his eyes and waited for an auditory cue which was presented following a jittered delay of between 1300 and 1700 ms. During each scene trial, the participant had 3000 ms to construct a novel, vivid scene in their imagination based on the cue (e.g. "jungle"). Each counting trial involved mentally counting in threes from a given number cue (e.g. "forty") for 3000 ms (beginning after the instruction had ended).

2.2.4. Data acquisition

All measurements were made inside a magnetically shielded room, manufactured by Vacuumschmelze, comprising two layers of mu-metal and one of aluminium designed to limit environmental interference. The participant wore a 3D printed scanner-cast that accommodated 20 temporal lobe OPM sensors bilaterally and a single mouth OPM in its custom made holder. OPM data were sampled at 1200 Hz using a 16-bit national instruments A/D converter. Data were recorded in 3 contiguous blocks and concatenated resulting in a total of 73 scene, and 68 counting, trials, each of 3000 ms duration.

A bi-planar coil system (Holmes et al., 2018) was used, in conjunction with a reference array (comprising 4 OPMs placed immediately behind the participant), to cancel the mean background field (in three orthogonal directions) inside the MSR and its first order spatial derivatives(dBx/dBz, dBy/dBz, dBz/dBz) over a central volume of $40 \times 40 \times 40$ cm^3 (Boto et al., 2018; Tierney et al., 2018).

2.2.5. Data analysis

All OPM data were first acausally filtered 1–8 Hz using a 4th order Butterworth filter. The data were then epoched into 3 s blocks based on digitally recorded triggers. The reference OPM array, and its temporal derivatives (i.e., 8 channels) were then used to reduce the environmental noise from each scalp OPM channel in turn on a trial by trial basis by means of a linear regression. The design matrix of reference sensors was inverted using the pseudoinverse (pinv in matlab) and multiplied by the data to obtain weights that defined a linear combination of reference sensors that when subtracted from the data minimised the residual sum of squares.

In order to verify that the data from the mouth sensor was qualitatively consistent with those from the temporal lobes we constructed time-frequency spectrograms of the difference between scene and counting trials at each sensor. We used the field-trip ((Oostenveld et al., 2011), http://www.fieldtriptoolbox.org/) based multi-taper spectral estimate method (spm_eeg_specest_ft_mtmconvol.m) over 1–8 Hz and 0–3000 ms. We then used a paired sample *t*-test to compare between time-frequency bins in the two conditions of interest.

Based on our previous cryogenic MEG experiment using the same stimuli (Barry et al., 2019a) we had a single hippocampal-specific time

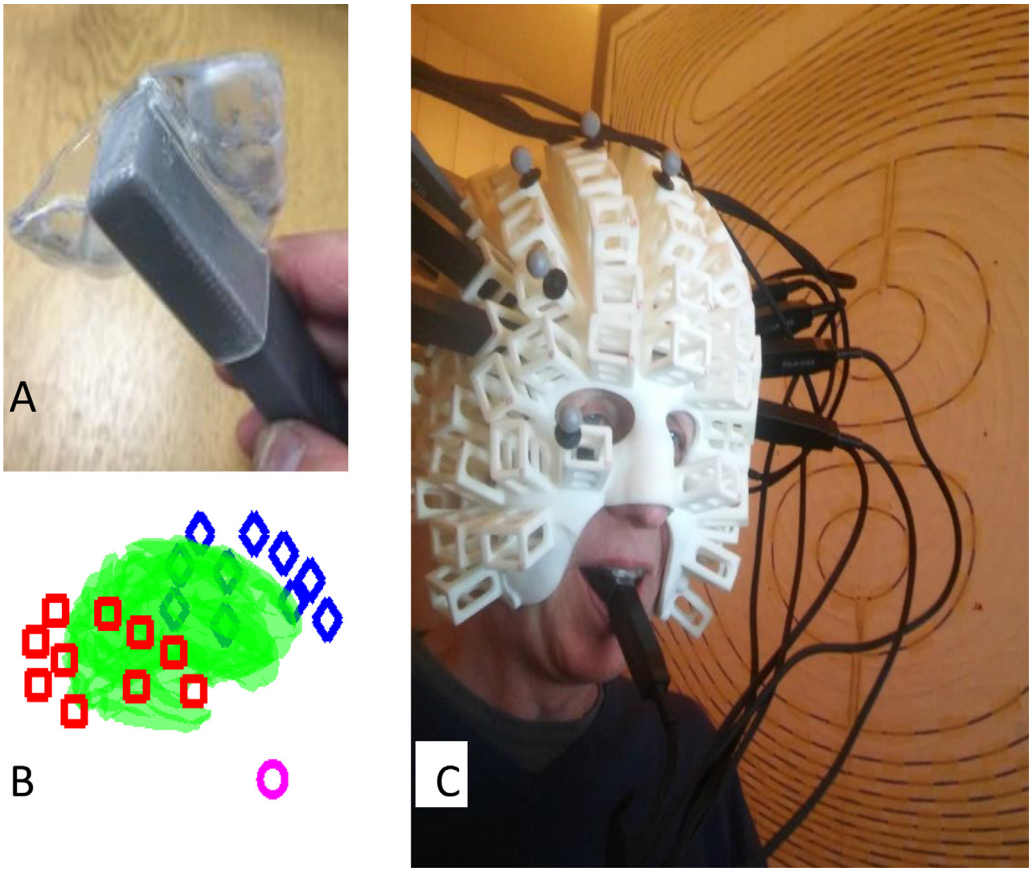

Fig. 1. Experimental set-up. **A.** The custom translucent thermoplastic intraoral sensor holder to encapsulate the end of a Quspin Gen 1 sensor (grey). **B.** Distribution of the sensors with respect to the participant's cortex (green). The mouth sensor is shown as a pink circle, right and left temporal lobe sensors are shown as red boxes and blue diamonds, respectively. **C.** The participant wearing a scanner-cast with the temporal lobe OPM array and the mouth sensor. Each individual scalp sensor is oriented normal to the scalp.

frequency window of interest of 0–3000 ms and 4–8 Hz (theta power-obtained from 5th order acausal Butterworth filter). At the sensor level we tested for the anticipated change in theta power between the 0 and 3000 ms post-stimulus windows in counting and scene conditions. Data from each trial and channel were windowed with a Hann window and band-pass filtered from 4 to 8 Hz. We used a paired-sample *t*-test to look for power change between scene trials and counting trials (68 of each in order to equalise the comparison).

All subsequent processing was carried out in SPM (https://www.fil.ion.ucl.ac.uk/spm/) or DAISS (https://www.fil.ion.ucl.ac.uk/spm/ext/#DAiSS). We performed the same contrast (scene versus counting, 4–8 Hz, 0–3000 ms) at the source level (grid spacing 5 mm) using an LCMV beamformer with automated Minka truncation (Minka, 2000) to produce volumetric whole-brain images (Supplementray Fig. S2). Minka truncation computes the model evidence under the Laplace approximation for a given data covariance and matrix selects the rank that maximises the model evidence. This approach is conceptually very similar to the use of variational free energy in SPM to optimise covariance components in source reconstruction (Friston et al., 2008; Lopez et al., 2014). We used the multivariate implementation of the LCMV beamformer in DAISS to perform this univariate test. This returns a classical F statistic (which we report here) in the univariate case. In order to look for MEG sensors making the greatest impact at the hippocampus, we systematically removed one MEG sensor at a time from the analysis and calculated the mean F statistic within this structure. Channels that have a positive impact on the hippocampal source reconstruction should give rise to a greater drop in the F-statistic (or variance explained in this structure) when removed.

Finally, we used a Dynamic Imaging of Coherent sources (DICs) beamformer with the mouth sensor (excluded from the source reconstruction) as the reference signal in order to create mouth-brain coherence images during the scene imagination condition (Coherence in the counting condition is provided in supplementary Fig. S3). Covariance and coherence windows were 0–3000 ms post cue onset, bandwidth was 4–8 Hz and the grid spacing was 5 mm. We note that a number of other studies in the area of episodic and spatial memory observe power changes in the 1–4 Hz band (Watrous et al., 2011; Lega et al., 2012; Pacheco Estefan et al., 2019) but we explicitly kept both the time window and frequency band the same as we have in our previous studies (Barry et al., 2019b). However, we provide supplementary analysis of this band in Fig. S1. The resulting images were then smoothed to 15 mm. In order to establish a significance threshold, we shuffled the mouth sensor trial data (with respect to the temporal channel data) and produced 100 (smoothed) coherence null images. Taking the maximum from each image established a null distribution which resulted in a coherence threshold corresponding to $p < 0.01$ (whole-volume corrected).

3. Results

3.1. Fields due to hippocampal generators

We first explored the sensitivity of all possible extra-cranial recording positions to sources on the hippocampal envelope. The SPM-extracted scalp mesh covered the external scalp contours and was a closed-form, approximately elliptical, structure. The mesh passed below the occiput, travelled through the base of the spine and, following the roof of the mouth, emerged onto the scalp surface once again at the

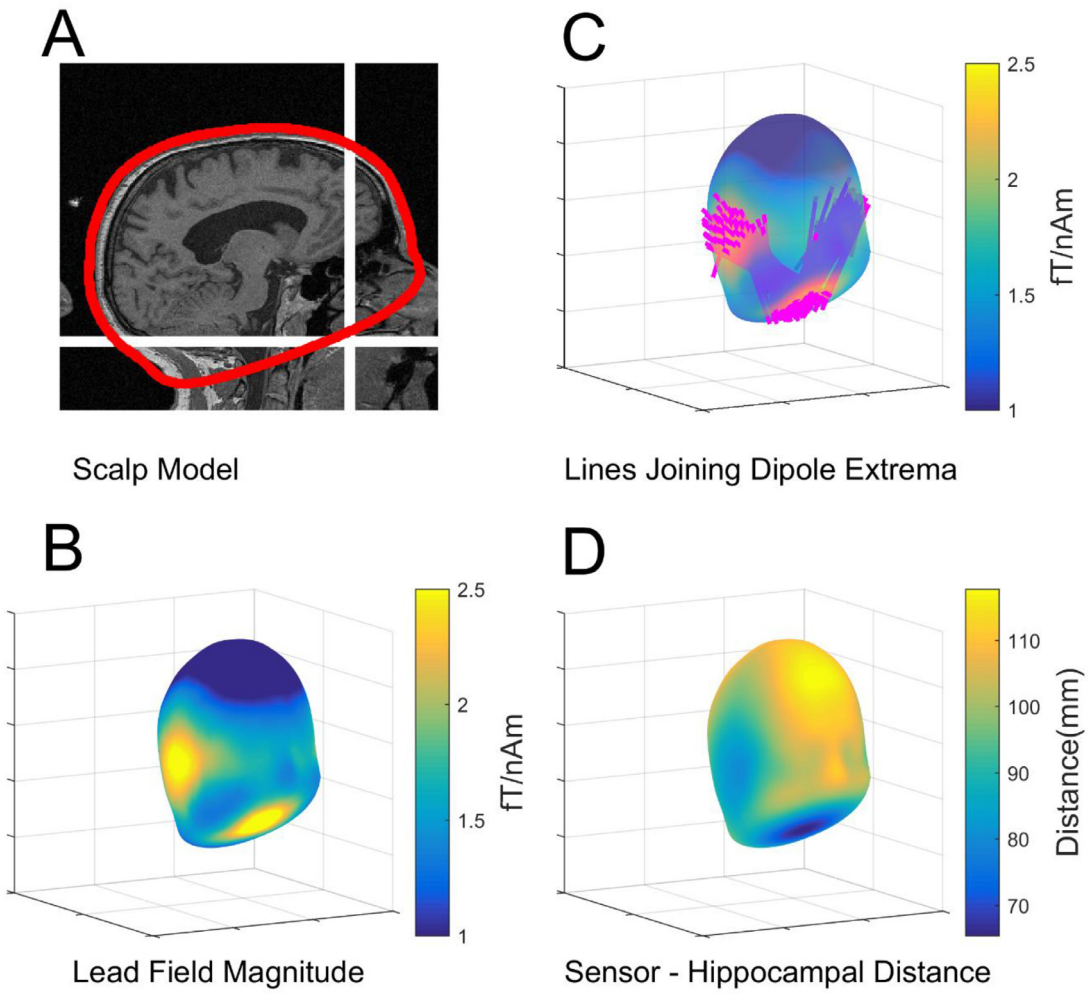

Fig. 2. Exploring the lead-field pattern due to hippocampal sources. **A.** Sagittal section from the MRI brain scan of the participant showing the SPM-extracted scalp mesh (red) and its path along the roof of the mouth. The location of mouth sensor is shown by white cross-hairs. **B.** The average field magnitude due to hippocampi on a shell displaced 6.5 mm from the scalp surface. Note the extrema at the temporal lobes and the roof of the mouth. **C.** The lines joining all field extrema for all hippocampal current elements. Note the clear pattern, with each hippocampal source giving rise to maximal (and opposing) field changes on one temporal lobe and the roof of the mouth. **D** The hippocampal to scalp distance is plotted on the scalp surface.

approximate level of the nasion (Fig. 2A). Based on sequentially positioning dipolar sources along this hippocampal model, we calculated the field magnitude at points on a shell displaced 6.5 mm from (and normal to) the scalp surface as an estimate of measurable OPM signal (Fig. 2B). Note that the base of the shell approximately corresponds to the roof of the mouth.

It is clear from Fig. 2B that the hippocampal generators gave rise to a large field magnitude on the temporal lobes, but also at the roof of the mouth. It is instructive to examine the lines joining positive and negative field extrema due to each hippocampal dipolar source. In Fig. 2C each hippocampal lead field maximum and minimum is in turn connected with a line. It is striking that the hippocampi generated fields that had extrema on the left and right temporal lobes (for left and right hippocampi respectively) also have additional (anti-correlated) companion extrema at the roof of the mouth. In Fig. 2D the distances from the hippocampus to roof of the mouth and scalp are shown.

3.2. Empirical recordings

Based on the simulations described above, we proceeded to test the feasibility of taking measurements from within the mouth cavity while the participant performed the hippocampal-dependant scene imagination task (Barry et al., 2019b).

Fig. 3 shows the sensor level data. Panels A-C show that the mouth sensor recordings are qualitatively similar to the temporal lobe channels suggesting that we have access to neuronal (rather than tongue or other artefactual) recordings.

Fig. 4A shows the channel-level t-statistical power changes between scene imagination and counting conditions based on our prior hypothesis (4–8 Hz, 0–3000 ms (Barry et al., 2019a). Note that the largest absolute t-statistic ($t = 3.08$, df = 134, $p < 0.0025$) occurred at the mouth sensor. The fact that this sensor, out of 21 sensors in total, showed the largest change is unlikely to have occurred by chance ($p < 0.0476$). This suggests that, not only is the mouth sensor picking up useful signal, but this signal is strongly modulated by a stimulus we know engages the hippocampus.

We then constructed a beamformer image of the contrast between scene imagination and counting (again over a 3 s window in the 4–8 Hz band). In order to identify channels key to explaining experimental variance within the hippocampus, we re-ran the beamformer reconstruction, but each time omitted one of the measurement sensors. Channels which were key to explaining experimental variance should give rise to lower F-statistic when omitted. Fig. 4B shows that the sensor that had the greatest impact on the amount of experimental variance explained was a channel on the left temporal lobe (channel 4). The impact of the mouth sensor on this analysis was modest (~10%). The fact that we observed

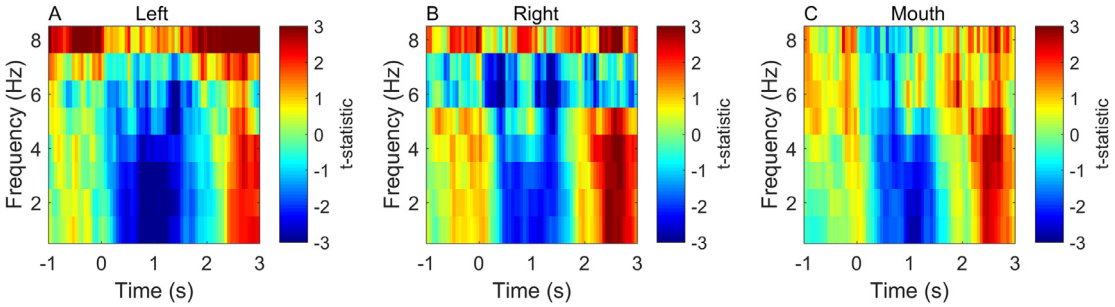

Fig. 3. Initial sensor level validation. Panels **A** and **B** show time-frequency spectrograms (1–8 Hz, −1 −3 s) of the t-statistical difference between scene and counting conditions for representative left, right temporal channels. Panel **C** shows the same contrast at the mouth sensor. The magnitude of the change in signal between conditions was approximately 30–60 fT.

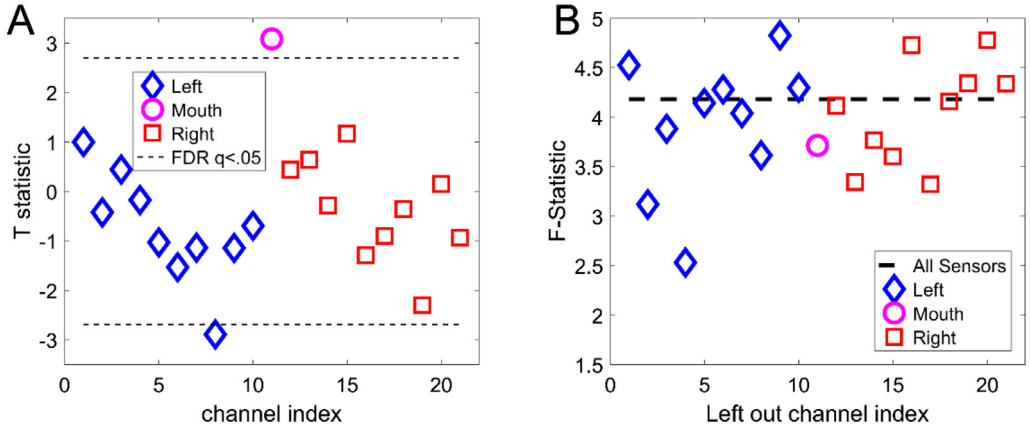

Fig. 4. Channel-specific tests at sensor and source level. The mouth sensor, left, and right temporal lobe channels are depicted as a pink circle, blue triangles and red squares respectively. **A.** Sensor-level two-sample tests on the theta power difference between scene imagination and counting trials. The largest task modulation (largest absolute t-statistic) is at the mouth sensor. Multiple comparisons are controlled for using FDR ($q < 0.05$) across sensors. **B.** F-statistic (relative power change) within the hippocampi when each measurement channel is excluded. The dotted line (baseline) indicates the F-statistic (power change) when using all channels. Removal of channels critical to the analysis should lead to a drop in power. Here we find that although the mouth sensor is important it is not as essential as some of the temporal lobe channels.

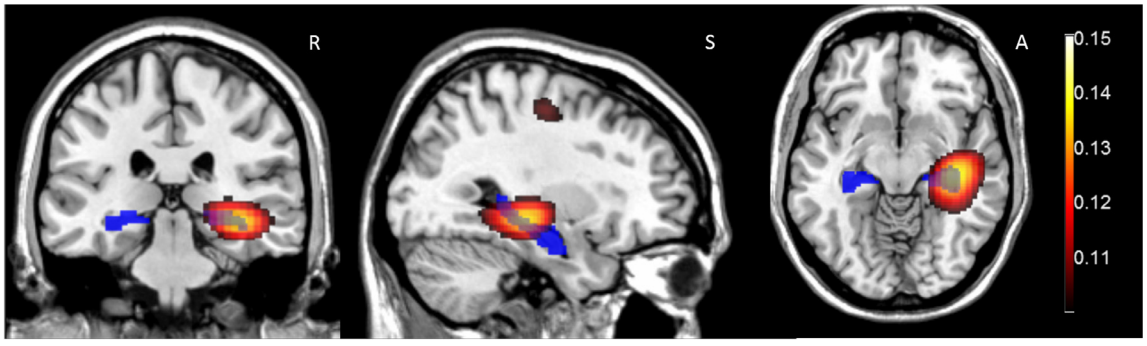

Fig. 5. Mouth sensor coherence (4–8 Hz) with the Beamformer reconstructed time series during the 'Scene' condition. Images are thresholded at FWE ($p < 0.05$). In the 4–8 Hz band the global coherence peak was found in the hippocampus (coherence=0.1527, $x = 36.00$ $y = -24.00$ $z = -8.00$). The AAL anatomical location of the hippocampi is shown in blue. Only two peaks are significant, the largest in the right hippocampus (on which the images are centred). The secondary peak (36.00–16.00 54.0) is at the border of primary motor cortex and BA6. Right, Superior and Anterior are indicated by R, S and A in the figure.

maximal experimental modulation at the mouth sensor, but that it made a small contribution to the source imaging, suggested to us that the lead-fields for that sensor might be in error (see discussion). To further probe whether or not the signal from the mouth sensor was coming from the hippocampus we used DICs. This allowed us to identify which brain regions were most coherent with the mouth sensor. The advantage of this analysis is that it does not require an explicit sensitivity profile (or lead field), for the mouth sensor.

Fig. 5 shows the DICs image of coherence between the mouth sensor and the beamformer source locations throughout the brain. We found the greatest coherence between the mouth sensor and source time-series within the beamformer image to be located in the right hippocampus (this was the global image maximum). Only one other peak survived the whole volume statistical correction ($p < 0.01$) and this bordered primary motor and Brodmann Area 6.

4. Discussion

We showed through simulation and empirical recordings that the inclusion of a mouth sensor could supplement and extend the growing literature on MEG measurements of the hippocampus (Pu et al., 2018; Pizzo et al., 2019; Ruzich et al., 2019). The simulation predicted an enhanced sensitivity to hippocampal generators within the mouth and we have provided the first demonstration of a mouth sensor's selectivity, both spectrally (Fig. 4A) and spatially (Fig. 5), to the human hippocampus.

We were initially surprised by the insights from the simulation study which clearly identified the roof of the mouth as the site of magnetic field extrema due to sources at the hippocampal surface. However, there are clear parallels here with the use of sphenoidal electrodes in EEG (Jones, 1951; Pampiglione and Kerridge, 1956) to access the base of the brain. Our simulation also suggested that each hippocampus should produce a unilateral temporal lobe extremum in conjunction with that found in the mouth. Reassuringly, recent simultaneous intracerebral electrophysiological and MEG recordings (Pizzo et al., 2019) have led to similar observations, with the invasively recorded hippocampal source giving rise to a strong, yet unilateral, temporal lobe signal. One interesting implication of the lead field modelling presented in the current study is the possibility of lead field cancellation in the mouth. If the currents generated in both hippocampi are positively correlated (and mirror symmetric) then some field cancellation will occur. Conversely, if both hippocampi are negatively correlated then an increase in signal would be observed in the mouth. In either case, additional mouth sensor(s) should help resolve the underlying physiology.

The hippocampus is the target of the majority of adult epilepsy surgeries (Margerison and Corsellis, 1966; Walker, 2015) and is heavily implicated in the progression of several forms of dementia (Huijbers et al., 2015; Buzsáki, 2015). This vulnerable brain structure is, therefore, an important focus for any non-invasive clinical imaging system. However, the main sensitivity benefit of OPMs over SQUID MEG systems is cortically focussed, with idealised sensitivity gains falling from five-fold cortically to two-fold for deeper structures (Boto et al., 2016; Iivanainen et al., 2017). Our findings show that mouth-based sensor arrays for MEG could potentially further enhance sensitivity to deep structures like the hippocampus.

Clinically, the ability to estimate electrical activity from the hippocampus non-invasively using mouth-based arrays would pose a much reduced risk compared to the surgical implantation of electrodes within the hippocampus, which is currently best-practice in cases when the source of the seizure focus is uncertain. Eliminating the need for this additional operation could significantly shorten the pathway to surgery to remove the aberrant seizure-inducing tissue. This study employed Gen 1 Quspin sensors and we only made use of measurements from one axis (axial to the sensor body). At present, the set-up needed to use an intraoral OPM sensor is cumbersome and uncomfortable; however, OPMs are continuing to decrease in size (Alem et al., 2014; Osborne et al., 2018). We hope that with improved sensor technology (and possibly by measuring a field from two orthogonal directions simultaneously) small mouth-based arrays might be possible in future.

Here we found that although the mouth sensor explained the most experimental variance (Fig. 4A) it was not the most important sensor for the source level analysis (Fig. 4B). A possible explanation for this is that the lead-fields for the mouth sensor may have been sub-optimal. The sensor position and orientation were estimated by visual inspection and could be in error by around 1 cm. Furthermore, it was not possible to orient the sensitive axis of the sensor in the mouth at the same angle used in the simulations (approximately 30° offset). In future studies, this could be improved by utilizing the additional measurement orientation offered by many OPMs (axial as well as tangential to the sensor body) to obtain better sampling of brain signals recorded using intraoral sensors. However, this is not the only potential source of of error in the lead-field modelling. We utilised the Nolte single shell model (2003) for our forward model as a compromise between accuracy and simplicity but this method has not been used before to model a sensor in the mouth. It is possible that the surrounding tissues (soft, hard pallet, sphenoid sinus) do not represent piecewise homogenous conductors necessitating that their conductivity should be explicitly modelled. The smoothness of the mouth surface could also affect the spatial frequency content of the signal with rougher surfaces necessitating the use of higher order spherical harmonics to be effectively modelled by the single shell method (Nolte, 2003). Clearly, more work in this area is required if the intraoral sensors are to be fully leveraged in source reconstruction.

In conclusion, we have demonstrated the feasibility of acquiring meaningful data using a scalp-array of OPM sensors augmented by an intraoral sensor. This intraoral sensor provides higher signal to noise than the temporal lobe sensors and is most coherent with the signal in the hippocampus. These results illustrate the potential that this approach holds for interrogating deep structures like the hippocampus in basic science and clinical studies.

Credit statement

Tim M. Tierney: Investigation, software, writing, visualization. **Andrew Levy:** investigation, Resources. **Daniel N. Barry:** investigation, methodology. **Sofie S. Meyer:** investigation. **Yoshihito Shigihara:** conceptualization, methodology. **Matt Everatt:** Resources. **Stephanie Mellor:** writing, validation. **Jose David Lopez:** writing. **Sven Bestmann:** investigation. **Niall Holmes:** investigation, methodology. **Gillian Roberts:** investigation. **Ryan M Hill:** investigation. **Elena Boto:** investigation. **James Leggett:** investigation. **Vishal Shah:** methodology. **Matthew J. Brookes:** methodology, writing. **Richard Bowtell:** methodology, writing. **Eleanor A. Maguire:** conceptualization, writing, methodology. **Gareth R. Barnes:** investigation, conceptualization, software, writing.

Declaration of Competing Interest

The design for biplanar magnetic field compensation coils, as used in this study, has been patented by the University of Nottingham. V.S. is the founding director of QuSpin, the commercial entity selling OPM magnetometers. QuSpin built the sensors used here and advised on the system design and operation, but played no part in the subsequent measurements or data analysis. This work was funded by a Wellcome collaborative award to G.R.B, M.J.B. and R.B. which involves a collaborative agreement with QuSpin.

Acknowledgements

This work was supported by a Wellcome Collaborative award to G.R.B., M.J.B. and R.B. (203257/Z/16/Z, 203257/B/16/Z), and a Wellcome Principal Research Fellowship to E.A.M. (210567/Z/18/Z). The Wellcome Centre for Human Neuroimaging is supported by a Centre Award from Wellcome (203147/Z/16/Z). We would like to thank S4S for generously providing the sensor housing and their time free of charge. The scanner-casts were designed and built by Mark Lim at Chalk Studios Ltd.

Supplementary materials

Supplementary material associated with this article can be found, in the online version, at doi:10.1016/j.neuroimage.2020.117443.

References

Alem, O., Benison, A.M., Barth, D.S., Kitching, J., Knappe, S., 2014. Magnetoencephalography of epilepsy with a microfabricated atomic magnetrode. J. Neurosci. 34, 14324–14327.

Barry, D.N., Barnes, G.R., Clark, I.A., Maguire, E.A., 2019a. The neural dynamics of novel scene imagery. J. Neurosci. 39, 4375–4386.

Barry, D.N., Tierney, T.M., Holmes, N., Boto, E., Roberts, G., Leggett, J., Bowtell, R., Brookes, M.J., Barnes, G.R., Maguire, E.A., 2019b. Imaging the human hippocampus with optically-pumped magnetoencephalography. Neuroimage 203, 1–8.

Boto, E., Bowtell, R., Kruger, P., Fromhold, T.M., Morris, P.G., Meyer, S.S., Barnes, G.R., Brookes, M.J., 2016. On the potential of a new generation of magnetometers for MEG: a beamformer simulation study. PLoS ONE 11, 1–24.

Boto, E., Holmes, N., Leggett, J., Roberts, G., Shah, V., Meyer, S.S., Muñoz, L.D., Mullinger, K.J., Tierney, T.M., Bestmann, S., Barnes, G.R., Bowtell, R., Brookes, M.J., 2018. Moving magnetoencephalography towards real-world applications with a wearable system. Nature doi:10.1038/nature26147.

Boto, E., Meyer, S.S., Shah, V., Alem, O., Knappe, S., Kruger, P., Fromhold, T.M., Lim, M., Glover, P.M., Morris, P.G., Bowtell, R., Barnes, G.R., Brookes, M.J., 2017. A new generation of magnetoencephalography: room temperature measurements using optically-pumped magnetometers. Neuroimage 149, 404–414.

Buzsáki, G., 2015. Hippocampal sharp wave-ripple: a cognitive biomarker for episodic memory and planning. Hippocampus 25, 1073–1188.

Dale, A.M., Fischl, B., Sereno, M.I., 1999. Cortical surface-based analysis. Neuroimage 9, 179–194.

Friston, K., Harrison, L., Daunizeau, J., Kiebel, S., Phillips, C., Trujillo-Barreto, N., Henson, R., Flandin, G., Mattout, J., 2008. Multiple sparse priors for the M/EEG inverse problem. Neuroimage 39, 1104–1120.

Holmes, N., Leggett, J., Boto, E., Roberts, G., Hill, R.M., Tierney, T.M., Shah, V., Barnes, G.R., Brookes, M.J., Bowtell, R., 2018. A bi-planar coil system for nulling background magnetic fields in scalp mounted magnetoencephalography. Neuroimage 181, 760–774.

Huijbers, W., Mormino, E.C., Schultz, A.P., Wigman, S., Ward, A.M., Larvie, M., Amariglio, R.E., Marshall, G.A., Rentz, D.M., Johnson, K.A., Sperling, R.A., 2015. Amyloid-β deposition in mild cognitive impairment is associated with increased hippocampal activity, atrophy and clinical progression. Brain 138, 1023–1035.

Iivanainen, J., Stenroos, M., Parkkonen, L., 2017. Measuring MEG closer to the brain: performance of on-scalp sensor arrays. Neuroimage 147, 542–553.

Jones, D.P., 1951. The EEG society (the electroencephalographic society). Electroencephalogr. Clin. Neurophysiol. 3, 100–101.

Lega, B.C., Jacobs, J., Kahana, M., 2012. Human hippocampal theta oscillations and the formation of episodic memories. Hippocampus 22, 748–761.

Litvak, V., Mattout, J., Kiebel, S., Phillips, C., Henson, R., Kilner, J., Barnes, G., Oostenveld, R., Daunizeau, J., Flandin, G., Penny, W., Friston, K., 2011. EEG and MEG data analysis in SPM8. Comput. Intell. Neurosci. doi:10.1155/2011/852961.

Lopez, J.D., Litvak, V., Espinosa, J.J., Friston, K., Barnes, G.R., 2014. Algorithmic procedures for Bayesian MEG/EEG source reconstruction in SPM. Neuroimage 84, 476–487.

Margerison, J.H., Corsellis, J.A., 1966. Epilepsy and the temporal lobes. A clinical, electroencephalographic and neuropathological study of the brain in epilepsy, with particular reference to the temporal lobes. Brain 89, 499–530.

Mattout, J., Henson, R.N., Friston, K.J., 2007. Canonical source reconstruction for MEG. Comput. Intell. Neurosci. 2007, 1–10.

Meyer, S.S., Rossiter, H., Brookes, M.J., Woolrich, M.W., Bestmann, S., Barnes, G.R., 2017. Using generative models to make probabilistic statements about hippocampal engagement in MEG. NeuroImage 149 (January), 468–482.

Minka, T., 2000. Automatic choice of dimensionality for PCA, vol. 514. M.I.T Media Laboratory Perceptual Computing Section, pp. 1–16.

Nolte, G., 2003. The magnetic lead field theorem in the quasi-static approximation and its use for magnetoenchephalography forward calculation in realistic volume conductors. Phys. Med. Biol. 48, 3637–3652.

Oostenveld, R., Fries, P., Maris, E., Schoffelen, J.-M., 2011. FieldTrip: open source software for advanced analysis of MEG, EEG, and invasive electrophysiological data. Comput. Intell. Neurosci. 2011, 1–9.

Osborne, J., Orton, J., Alem, O., Shah, V., 2018. Fully integrated, standalone zero field optically pumped magnetometer for biomagnetism. Steep Dispers. Eng. Opto At. Precis. Metrol. 10548, 1–7.

Pacheco Estefan, D., Sánchez-Fibla, M., Duff, A., Principe, A., Rocamora, R., Zhang, H., Axmacher, N., Verschure, P.F.M.J., 2019. Coordinated representational reinstatement in the human hippocampus and lateral temporal cortex during episodic memory retrieval. Nat. Commun. doi:10.1038/s41467-019-09569-0.

Pampiglione, G., Kerridge, J., 1956. Abnormalities from the temporal lobe studied with sphenoidal electrodes. J. Neurol. Neurosurg. Psychiatry doi:10.1136/jnnp.19.2.117.

Pizzo, F., Roehri, N., Medina Villalon, S., Trébuchon, A., Chen, S., Lagarde, S., Carron, R., Gavaret, M., Giusiano, B., McGonigal, A., Bartolomei, F., Badier, J.M., Bénar, C.G., 2019. Deep brain activities can be detected with magnetoencephalography. Nat. Commun. 10, 1–13.

Pu, Y., Cheyne, D.O., Cornwell, B.R., Johnson, B.W., 2018. Non-invasive investigation of human hippocampal rhythms using magnetoencephalography: a review. Front. Neurosci. doi:10.3389/fnins.2018.00273.

Ruzich, E., Crespo-García, M., Dalal, S.S., Schneiderman, J.F., 2019. Characterizing hippocampal dynamics with MEG: a systematic review and evidence-based guidelines. Hum. Brain Mapp. 40, 1353–1375.

Tierney, T.M., Holmes, N., Meyer, S.S., Boto, E., Roberts, G., Leggett, J., Buck, S., Duque-Muñoz, L., Litvak, V., Bestmann, S., Baldeweg, T., Bowtell, R., Brookes, M.J., Barnes, G.R., 2018. Cognitive neuroscience using wearable magnetometer arrays: non-invasive assessment of language function. Neuroimage 181, 513–520.

Walker, M., 2015. Hippocampal sclerosis: causes and prevention. Semin. Neurol. 35, 193–200.

Watrous, A.J., Fried, I., Ekstrom, A.D., 2011. Behavioral correlates of human hippocampal delta and theta oscillations during navigation. J. Neurophysiol. 105, 1747–1755.